

# First-principles phase-coherent transport in metallic nanotubes with realistic contacts

J. J. Palacios,<sup>1</sup> A. J. Pérez-Jiménez,<sup>2</sup> E. Louis,<sup>1</sup> E. SanFabián,<sup>2</sup> and J. A. Vergés.<sup>3</sup>

<sup>1</sup>*Departamento de Física Aplicada, Universidad de Alicante,  
San Vicente del Raspeig, Alicante 03690, Spain.*

<sup>2</sup>*Departamento de Química-Física, Universidad de Alicante,  
San Vicente del Raspeig, Alicante 03690, Spain.*

<sup>3</sup>*Departamento de Teoría de la Materia Condensada,  
Instituto de Ciencias de Materiales de Madrid (CSIC), Cantoblanco, Madrid 28049, Spain.*

(Dated: March 22, 2022)

We present first-principles calculations of phase coherent electron transport in a carbon nanotube (CNT) with realistic contacts. We focus on the zero-bias response of open metallic CNT's considering two archetypal contact geometries (end and side) and three commonly used metals as electrodes (Al, Au, and Ti). Our *ab-initio* electrical transport calculations make, for the first time, quantitative predictions on the contact transparency and the transport properties of finite metallic CNT's. Al and Au turn out to make poor contacts while Ti is the best option of the three. Additional information on the CNT band mixing at the contacts is also obtained.

Controversy on the observed electrical transport properties of carbon nanotubes (CNT's) has been mostly due to our lack of control and understanding of their contact to the metallic electrodes. It has finally become clear that the contact influences critically the overall performance of the CNT and that it is crucial to lower the inherent contact resistance to achieve the definite understanding of the intrinsic electrical properties of CNT's[1, 2, 3]. In order to determine the relevant factors behind the contact resistance so that this can be pushed down to its alleged quantum limit  $R_0 = h/2e^2$  per CNT channel a big experimental effort has been made both in CNT growth and lithographic techniques[4, 5, 6, 7, 8, 9, 10]. While considerable progress in this direction has already been achieved, theoretical progress, on the other hand, lags behind in this important issue.

The actual atomic structure of the electrode (and probably that of the CNT) at the contact are unknown and, most likely, change from sample to sample when fabricated under the same conditions. Atomic-scale modeling, however, can still be of guidance to the interpretation of the experiments and to the future design of operational devices with CNT's. In this work we focus on the two key ingredients in this puzzle: The effect the atomic-scale geometry and the chemical nature of the electrode have on the transparency of the contact. We have studied open single-walled metallic (5,5) CNT's contacted in two representative forms (see Fig. 1) to Al, Au, and Ti electrodes which are among the most commonly used metals in the experiments. From our *ab-initio* transport study we find that in CNT's contacted to Al and Au electrodes for end-contact geometry [see Fig. 1(a)] the two CNT bands couple weakly to the electrodes. This allows us to resolve quasi-bound CNT states in the conductance and to estimate the magnitude of the degeneracy removal due to Coulomb blockade effects in a direct manner. Moreover, we find that the two bands couple very differently to the electrodes (one of them is almost shut down for

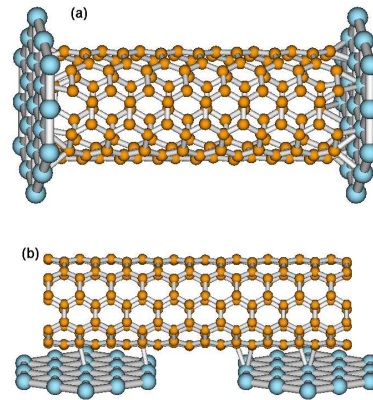


FIG. 1: The two contact geometries considered in this work: An open (5,5) carbon nanotube end-contacted to (111) surfaces (a) and the same nanotube side-contacted (b).

transport) and do not mix. For the side-contact geometry [see Fig. 1(b)] the coupling is the same for both bands, but similar in strength to the end-contact geometry. Finally, our study presents the first direct numerical evidence of what has been hinted at on the basis of indirect first-principles calculations[11, 12] and what has recently been observed in experiments[7]: Early 3-*d* elements as Ti are probably the best choice for making high-transparency contacts to CNT's compared to more traditional metals such as Al and Au. Although perfect transparency at the contact is never achieved, our calculations indicate that properly engineered Ti contacts are a good bet for future perfect contacts to CNT's.

From a theory point of view, the “contact” problem has been previously addressed[10, 13, 14], but only partially. The reason is that a full analysis of this problem requires the use of sophisticated state-of-the-art numerical techniques to calculate electrical transport from first-principles[15, 16, 17], where even the electrodes need to

be described down to the atomic level[18, 19, 20, 21, 22]. These techniques are currently under development. First of all, charge transfer at the contact, which aligns the chemical potentials of the electrodes and the CNT, needs to be evaluated self-consistently[23, 24]. Secondly, one needs to combine the *ab-initio* calculation with Landauer's formalism[25]. Recently, we have presented a very promising approach, termed Gaussian Embedded Cluster Method[20, 21], that allows us to address this problem in its full complexity. Our method is based on standard quantum chemistry calculations performed with the Gaussian98 code[26]. A density functional (DF) calculation of a cluster comprising the CNT and a significant part of the electrodes is performed (see Fig. 1). Next, the retarded(advanced) Green's functions associated with the self-consistent hamiltonian or Fock operator  $\hat{F}$  of the cluster is modified to include the rest of the semi-infinite electrodes:

$$\left[ (E \pm i\delta) - \hat{F} - \hat{\Sigma}^{(\pm)} \right] \hat{G}^{(\pm)} = \hat{I}. \quad (1)$$

In this expression  $\hat{\Sigma}^{(\pm)} = \hat{\Sigma}_R^{(\pm)} + \hat{\Sigma}_L^{(\pm)}$ , where  $\hat{\Sigma}_R$  ( $\hat{\Sigma}_L$ ) denotes a self-energy operator that accounts for the part of the right(left) semi-infinite electrode that has not been included in the initial DF calculation[29], and  $\hat{I}$  is the unity matrix. In a non-orthogonal basis, like those commonly used in Gaussian98, the embedded cluster density matrix takes the form

$$P = -\frac{1}{\pi} \int_{-\infty}^{E_F} \text{Im} \left[ S^{-1} G^{(-)}(E) S^{-1} \right] dE, \quad (2)$$

where  $S$  is the overlap matrix,  $G^{(-)}$  is the retarded Green's function expressed in the non-orthogonal basis, and  $E_F$  is the Fermi energy which is set by imposing overall charge neutrality in the cluster. The density matrix is returned to Gaussian98 and the process is repeated until the procedure converges. The conductance can finally be calculated through the standard expression[25]:

$$\mathcal{G} = \frac{2e^2}{h} \text{Tr}[T] = \frac{2e^2}{h} \text{Tr}[\Gamma_L G^{(-)} \Gamma_R G^{(+)}], \quad (3)$$

where  $\text{Tr}$  denotes the trace over all the orbitals in the cluster and where the matrices  $\Gamma_R$  and  $\Gamma_L$  are  $i(\Sigma_R^{(-)} - \Sigma_R^{(+)})$  and  $i(\hat{\Sigma}_L^{(-)} - \hat{\Sigma}_L^{(+)})$ , respectively. In order to single out the contribution of individual channels to the current one can diagonalize the transmission matrix  $T$ .

Figure 2(a) shows  $\mathcal{G}$  around the Fermi energy for a (5,5) metallic CNT composed of  $N = 10$  carbon layers that has been end-contacted [Fig. 1(a)] to Al(111) surfaces (the end-carbon-layer-surface distance has been optimized to a value of 1.8 Å)[30]. Four resonances appear around the Fermi energy (set to zero). These resonances can be easily traced back to four extended states of the isolated finite CNT[24]. Two of them ( $k_1, k_2$ ) originate in the bonding ( $\pi$ ) band of the CNT and the other two ( $k_1^*, k_2^*$ )

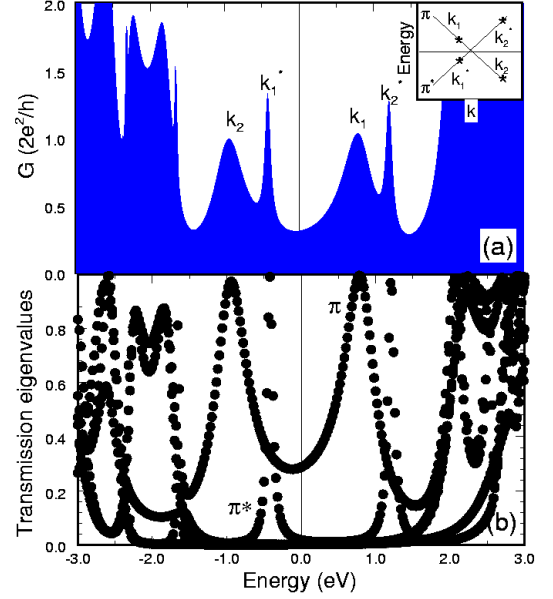


FIG. 2: (a) Conductance as a function of energy for an  $N = 10$  (5,5) open metallic nanotube end-contacted to a Al(111) surface [see Fig. 1(a)]. The nanotube-surface distance has been optimized to a value of 1.8 Å and the Fermi energy is set to zero. Inset: Schematic band structure of the metallic nanotube showing the four states responsible for the resonances. (b) Transmission as a function of energy for the highest conducting channels. The symmetry of the two main channels is also shown.

in the antibonding ( $\pi^*$ ) band (see inset in Fig. 2). The resonances have different widths for different bands indicating that they couple very differently to the electrodes. Moreover, the two bands do not mix with each other. This is more clearly seen in Fig. 2(b) where we show the highest transmission eigenvalues of the transmission matrix. Two independent channels exhibit resonances in the energy window ( $\approx 3.5\text{eV}$ ) around  $E_F$  where only the  $\pi$  and  $\pi^*$  bands can contribute to transport. This result is consistent with the fact that  $\pi^*$  states, of large angular momentum, do not couple to the low-angular momentum states of the electrode, while  $\pi$  states, of low angular momentum, couple more easily[13, 14]. Notice that there is a charge transfer from the metal to the CNT, but this mainly localizes at the end carbon layer ( $\approx 0.2$  per carbon atom) and it does not affect the overall band positioning in the center of the CNT.

The specific band assignment of the resonances is nicely confirmed by their evolution on the length of the CNT presented in Fig. 3. We have calculated the conductance for  $N = 8, 9, 10, 11, 12$ , and 13 carbon-layer CNT's. The opposite signs of the group velocity for the  $\pi$  and  $\pi^*$  bands make the quasi-bound states belonging to the  $\pi$  band shift down in energies while those belonging to the  $\pi^*$  band shift up as  $N$  increases. As expected from a simple

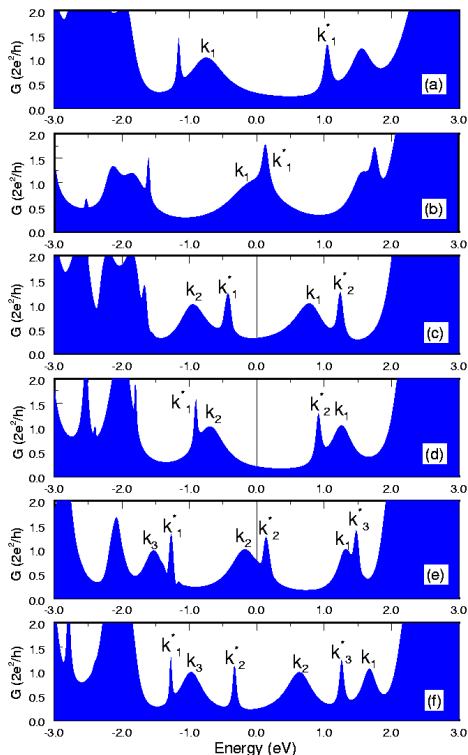


FIG. 3: Conductance as a function of energy for an  $N = 8$ (a),  $N = 9$ (b),  $N = 10$ (c),  $N = 11$ (d),  $N = 12$ (e), and  $N = 13$ (f) (5,5) open metallic nanotube end-contacted to a Al(111) surface [see Fig. 1(a)]. The Fermi energy has been set to zero.

particle-in-a-box argument applied to finite CNT's[24], for  $N = 3l$ , where  $l$  is an integer, we should expect two states with the same wave vector  $k_n$  but in different bands to coincide at the Fermi energy. Naively one should thus expect  $\mathcal{G} = 4e^2/h$ [27]. Our results for the contacted  $N = 9$  and  $N = 12$  CNT's show otherwise: Two resonances never coincide at the Fermi level. The reason is that Coloumb blockade prevents two (band and/or spin) degenerate quasibound states to be filled up at the same time and degeneracies are removed[31]. From Figs. 3(b) and (e) we estimate the charging energy to be  $\approx 0.3$  eV in these CNT's which is smaller than the single-particle level spacing as confirmed by experiments[9].

If the interpretation of the different coupling strengths of the CNT bound states with the Al electrodes is correct and angular momentum considerations are relevant, similar couplings should be expected for both bands if no axial symmetry is present. This is the case for the other contact geometry considered in this work [see Fig.1(b)]. Figure 4 shows results for an  $N = 15$  CNT side-contacted to Al(111) surfaces (the CNT-surface distance has been optimized to  $2.3\text{\AA}$ ). Conductance resonances come in pairs in the relevant energy window which is what is

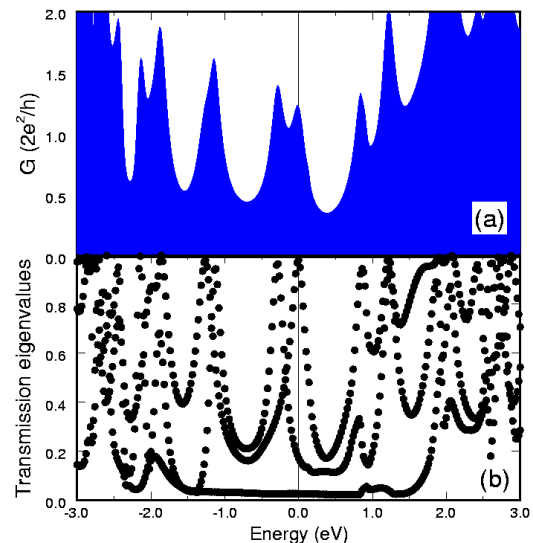


FIG. 4: (a) Conductance as a function of energy for an  $N = 15$  (5,5) open metallic nanotube side-contacted to a Al(111) surface [see Fig. 1(b)]. The nanotube-surface distance has been optimized to a value of  $2.2\text{\AA}$ . (b) Transmission as a function of energy for the three highest conducting channels.

expected for an  $N = 15$  CNT. More importantly, all of them present similar widths, confirming our expectations. Contrary to the previous geometry, localized end states[24] influence the coupling around  $1\text{eV}$  for this contact geometry where mixing with the CNT extended states takes place. Our results for the coupling strength with Al contacts are consistent with previous studies where jellium models were considered as contacts[14], and with those in Ref. 18, but we do not subscribe previous *ab-initio* results presented in Ref. 28 based on what it seems to be more realistic contact models similar to ours.

We now complete our study for end-contacted  $N = 10$  CNT's considering Au and Ti electrodes (see Figs. 5 and 6). Several resonances are clearly visible close to the Fermi energy for the case of Au, but, in contrast to Al electrodes, it is difficult to identify specific extended states as we did above. This is in part due to the mixing of the  $\pi$  and  $\pi^*$  bands with the end states which, in addition, induce extra channels in the conductance, although these channels are only relevant for transport in very short CNT's[32]. Apart from this, the coupling strength of the two bands is similar to that found for Al electrodes despite of the fact that the Mulliken population analysis reflects a minor charge transfer from the electrode to the CNT. In Fig. 5(b) we appreciate that the  $\pi$  band coupling is also stronger than that of the  $\pi^*$  band. In contrast to Al and Au electrodes, where  $\mathcal{G}$  exhibits resonances,  $\mathcal{G}$  presents an oscillatory behavior for Ti around  $E_F$ . This is accompanied, as the anticross-

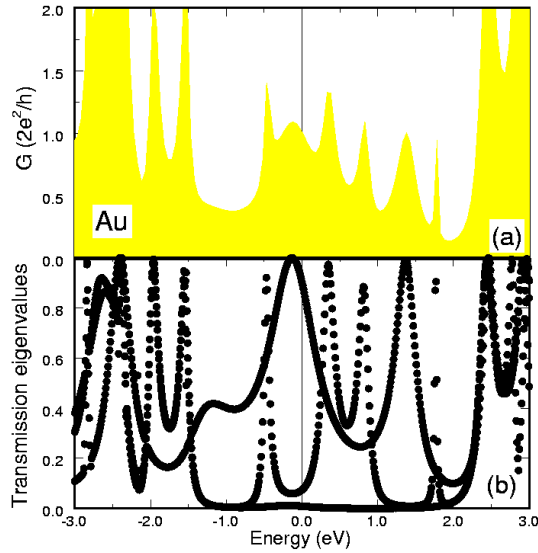


FIG. 5: (a) Conductance as a function of energy for an  $N = 10$  (5,5) open metallic nanotube end-contacted to a Au(111) surface [see Fig. 1(a)]. The nanotube-surface distance has been optimized to a value of 2.2 Å. (b) Transmission as a function of energy for the highest conducting channels.

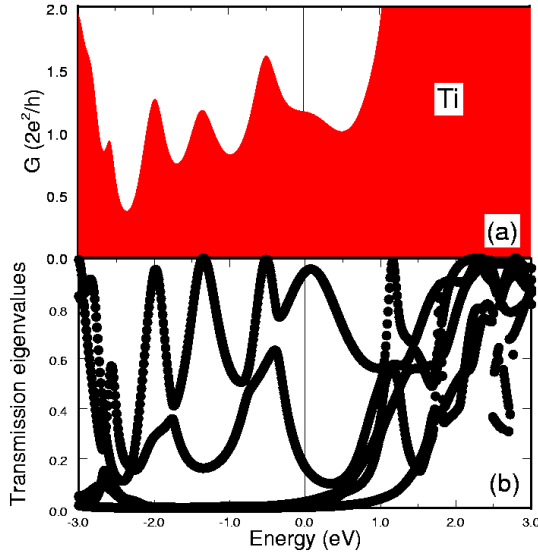


FIG. 6: (a) Conductance as a function of energy for an  $N = 10$  (5,5) open metallic nanotube end-contacted to a Ti(111) surface [see Fig. 1(a)]. The nanotube-surface distance has been optimized to a value of 1.8 Å. (b) Transmission as a function of energy for the highest conducting channels.

ings in the transmission eigenvalues reveal in Fig. 6(b), by band mixing. This result reflects, as suggested in Ref. 12, that Ti couples differently to the CNT (due to the presence of  $d$ -states at the Fermi energy) and forms a better contact (the charge transfer is  $\approx 0.4$  electrons per

C atom at the end layer). At this point, however, we can only speculate on the possibility of perfect transparency for other Ti electrode geometries.

We acknowledge support by the Spanish CICYT under Grant No. 1FD97-1358 and by the Generalitat Valenciana under Grants No. GV00-151-01 and GV00-095-2. J.J.P. thanks S. Y. Wu for encouraging this work in its initial stages.

- 
- [1] S. Frank, P. Poncharal, Z. L. Wang, and W. A. de Heer, *Science* **280**, 1744 (1998).
  - [2] A. Bachtold, M. S. Fuhrer, S. Plyasunov, M. Forero, E. H. Anderson, A. Zettl, and P. L. McEuen, *Phys. Rev. Lett.* **84**, 6082 (2000).
  - [3] J. Nygard, D. H. Cobden, and P. E. Lindelof, *Nature (London)* **408**, 342 (2000).
  - [4] H. T. Soh, C. F. Quate, A. F. Morpurgo, C. M. Marcus, J. Kong, and H. Dai, *Appl. Phys. Lett.* **75**, 627 (1999).
  - [5] C. Zhou, J. Kong, and H. Dai, *Phys. Rev. Lett.* **84**, 5604 (2000).
  - [6] J. Appenzeller, R. Martel, P. Avouris, H. Stahl, and B. Lengeler, *Appl. Phys. Lett.* **78**, 3313 (2001).
  - [7] J. Kong, E. Yenilmez, T. W. Tombler, W. Kim, H. Dai, R. B. Laughlin, L. Liu, C. S. Jayanthi, and S. Y. Wu, *Phys. Rev. Lett.* **87**, 106801 (2001).
  - [8] A. Kanda, Y. Ootuka, K. Tsukagoshi, and Y. Aoyagi, *Appl. Phys. Lett.* **79**, 1354 (2001).
  - [9] W. Liang, M. Bockrath, and H. Park, *Phys. Rev. Lett.* **88**, 126801 (2002).
  - [10] V. Derycke, R. Martel, J. Appenzeller, and P. Avouris, *Appl. Phys. Lett.* **80**, 2773 (2002).
  - [11] A. N. Andriotis, M. Menon, and G. E. Froudakis, *Appl. Phys. Lett.* **76**, 3890 (2000).
  - [12] C. K. Yang, J. Zhao, and J. P. Lu, *Phys. Rev. B* **66**, 041403 (2002).
  - [13] H. J. Choi, J. Ihm, Y.-G. Yoon, and S. G. Louie, *Phys. Rev. B* **60**, R14009 (1999).
  - [14] M. P. Anantram, *Appl. Phys. Lett.* **78**, 2055 (2001).
  - [15] N. D. Lang, *Phys. Rev. B* **53**, 5335 (1995).
  - [16] S. N. Yaliraki and M. A. Ratner, *J. Chem. Phys.* **109**, 5036 (1998).
  - [17] P. S. Damle, A. W. Ghosh, and S. Datta, *Phys. Rev. B* **64**, 201403 (2001).
  - [18] J. Taylor, H. Guo, and J. Wang, *Phys. Rev. B* **63**, 121104 (2001).
  - [19] J. Taylor, H. Guo, and J. Wang, *Phys. Rev. B* **63**, 245407 (2001).
  - [20] J. J. Palacios, A. J. Pérez-Jiménez, E. Louis, and J. A. Vergés, *Phys. Rev. B* **64**, 115411 (2001).
  - [21] J. J. Palacios, A. J. Pérez-Jiménez, E. Louis, E. San-Fabian, and J. A. Vergés, *Phys. Rev. B* **66**, 035322 (2002).
  - [22] M. Brandbyge, J. Taylor, M. Stokbro, J. L. Mozos, and P. Ordejón, *Phys. Rev. B* **65**, 165401 (2002).
  - [23] Y. Xue and S. Datta, *Phys. Rev. Lett.* **83**, 4844 (1999).
  - [24] A. Rubio, D. Sánchez-Portal, E. Artacho, P. Ordejón, and J. M. Soler, *Phys. Rev. Lett.* **82**, 3520 (1999).
  - [25] S. Datta, *Electronic transport in mesoscopic systems* (Cambridge University Press, Cambridge, 1995).

- [26] M. J. Frisch, G. W. Trucks, H. B. Schlegel, M. A. R. G. E. Scuseria, J. R. Cheeseman, V. G. Zakrzewski, J. A. Montgomery, Jr., R. E. Stratmann, J. C. Burant, et al., GAUSSIAN98, Revision A.7, Gaussian, Inc., Pittsburgh PA, 1998.
- [27] D. Orlikowski, H. Mehrez, J. Taylor, H. Guo, J. Wang, and C. Roland, Phys. Rev. B **63**, 155412 (2001).
- [28] M. B. Nardelli, J. L. Fattebert, and J. Bernholc, Phys. Rev. B **64**, 245423 (2001).
- [29] We choose to describe the bulk electrode with a Bethe lattice tight-binding model with the coordination and parameters appropriate for the electrodes[20, 21]. Details on the Bethe lattice parameters, the density functional, and the basis set used in our calculations can be found in Ref. 21.
- [30] A word of caution is due here. Within DF theory only  $\mathcal{G}(E_F)$  has a strict meaning. In order to obtain the zero-bias conductance at different energies which would correspond to the conductance for different values of an external gate potential which can charge or discharge the system, one must perform the self-consistent calculation for a varying Fermi energy. We have analyzed the extent of this problem and found that our conclusions are not modified significantly as the charge in the system varies. This partially justifies plotting  $\mathcal{G}(E)$  for neutral systems. However this problem might deserves a further consideration when bound or quasibound states are present in the CNT (see text below).
- [31] We have analyzed the Coulomb blockade process in detail for the  $N = 9$  CNT. For a partially discharged CNT the two resonances labeled  $k_1$  and  $k_1^*$  coincide in energy above the Fermi energy and the conductance reaches there  $4e^2/h$ . For the neutral [see Fig. 3(b)] or slightly charged system this degeneracy is partially removed and the conductance drops. The spin degeneracy removal due to Coulomb blockade requires technically challenging open shell calculations and is currently under study.
- [32] A detailed analysis of why the end states do not play a significant role for Al in end-contact geometries is deferred for future work.